








Article

Synergistic Effect of rhBMP-2 Protein and Nanotextured Titanium Alloy Surface to Improve Osteogenic Implant Properties

Andrea Mesa-Restrepo ^{1,2,*}, Ana Civantos ^{2,3}, Jean Paul Allain ^{2,3}, Edwin Patiño ⁴, Juan Fernando Alzate ⁵, Norman Balcázar ⁶, Robinson Montes ⁷, Juan José Pavón ⁷, José Antonio Rodríguez-Ortiz ⁸ and Yadir Torres ⁸

- ¹ Department of Biomedical Engineering, Pennsylvania State University, State College, PA 16802, USA
 - ² The Ken and Mary Alice Lindquist Department of Nuclear Engineering, Pennsylvania State University, State College, PA 16802, USA; ancife@illinois.edu (A.C.); allain@psu.edu (J.P.A.)
 - ³ Department of Nuclear, Plasma and Radiological Engineering, University of Illinois at Urbana-Champaign, Urbana, IL 61801, USA
 - ⁴ Structural Biochemistry of Macromolecules, Chemistry Institute, University of Antioquia, Medellín 50022, Colombia; edwin.patiño@udea.edu.co
 - ⁵ National Center for Genomic Sequencing-CNSG, School of Medicine, University of Antioquia, Medellín 50022, Colombia; jfernando.alzate@udea.edu.co
 - ⁶ Department of Physiology and Biochemistry, School of Medicine, University of Antioquia, Medellín 50022, Colombia; norman.balcazar@udea.edu.co
 - ⁷ Grupo de Biomateriales Avanzados y Medicina Regenerativa BAMR, Facultad de Ingeniería, Universidad de Antioquia, Medellín 50022, Colombia; robinson.montes@udea.edu.co (R.M.); juan.pavon@udea.edu.co (J.J.P.)
 - ⁸ Departamento de Ingeniería y Ciencia de los Materiales y del Transporte, Escuela Politécnica Superior, Universidad de Sevilla, 41003 Sevilla, Spain; jarortiz@us.es (J.A.R.-O.); ytorres@us.es (Y.T.)
- * Correspondence: aqm6463@psu.edu; Tel.: +1-2177213197



Citation: Mesa-Restrepo, A.; Civantos, A.; Allain, J.P.; Patiño, E.; Alzate, J.F.; Balcázar, N.; Montes, R.; Pavón, J.J.; Rodríguez-Ortiz, J.A.; Torres, Y. Synergistic Effect of rhBMP-2 Protein and Nanotextured Titanium Alloy Surface to Improve Osteogenic Implant Properties. *Metals* **2021**, *11*, 464. <https://doi.org/10.3390/met11030464>

Academic Editors: Asit Kumar Gain and Leszek Adam Dobrzanski

Received: 29 December 2020
Accepted: 9 March 2021
Published: 11 March 2021

Publisher's Note: MDPI stays neutral with regard to jurisdictional claims in published maps and institutional affiliations.



Copyright: © 2021 by the authors. Licensee MDPI, Basel, Switzerland. This article is an open access article distributed under the terms and conditions of the Creative Commons Attribution (CC BY) license (<https://creativecommons.org/licenses/by/4.0/>).

Abstract: One of the major limitations during titanium (Ti) implant osseointegration is the poor cellular interactions at the biointerface. In the present study, the combined effect of recombinant human Bone Morphogenetic Protein-2 (rhBMP-2) and nanopatterned Ti6Al4V fabricated with Directed irradiation synthesis (DIS) is investigated in vitro. This environmentally-friendly plasma uses ions to create self-organized nanostructures on the surfaces. Nanocones (≈ 36.7 nm in DIS 80°) and thinner nanowalls (≈ 16.5 nm in DIS 60°) were fabricated depending on DIS incidence angle and observed via scanning electron microscopy. All samples have a similar crystalline structure and wettability, except for sandblasted/acid-etched (SLA) and acid-etched/anodized (Anodized) samples which are more hydrophilic. Biological results revealed that the viability and adhesion properties (vinculin expression and cell spreading) of DIS 80° with BMP-2 were similar to those polished with BMP-2, yet we observed more filopodia on DIS 80° (≈ 39 filopodia/cell) compared to the other samples (< 30 filopodia/cell). BMP-2 increased alkaline phosphatase activity in all samples, tending to be higher in DIS 80° . Moreover, in the mineralization studies, DIS 80° with BMP-2 and Anodized with BMP-2 increased the formation of calcium deposits (> 3.3 fold) compared to polished with BMP-2. Hence, this study shows there is a synergistic effect of BMP-2 and DIS surface modification in improving Ti biological properties which could be applied to Ti bone implants to treat bone disease.

Keywords: surface modification; bone morphogenetic proteins; directed irradiation synthesis; nanopatterning; advanced biointerfaces; osseointegration

1. Introduction

Bone loss affects more than half a million patients in the United States and represents over \$2.5 billion in health costs. Indeed, trauma, tumor recessions or developmental defects limit bone's ability to self-repair after an injury, creating large non-healing fragments that require the necessary use of implants and other medical devices [1]. Current treatments

use bone metal implants based on titanium (Ti) and Ti-based alloys to replace a diversity of bone tissue, including dental implants, repair large bone defects, spinal bone implants, and a host of reconstructive and regenerative solutions for millions of patients. Ti and its alloys are widely used in the dentistry and orthopedic industry due to their excellent biological and chemico-mechanical properties. When Ti is exposed to air, it forms a passive oxide layer (TiO_2) that is responsible for its chemical inertness, corrosion resistance, and biocompatibility. Unfortunately, conventional Ti surfaces (polished) show a limited cellular interaction at the biointerface, limiting the formation of a strong direct chemical bond between implant and tissue, also known as osseointegration. During the implantation process, tissues are damaged, and an acute inflammation process occurs—if this becomes chronic, the implant is encapsulated in fibrotic tissue and finally is rejected [2–6]. Thus, there is an urgent need to improve titanium bone contact to accelerate healing times, avoid implant failure, and minimize secondary surgeries to remove it, reducing the associated costs and increasing the patient's quality of life [3,7,8].

Framed into this special issue, researchers from a multidisciplinary field (e.g., engineers, biologists, physicists, pharmacists) have joined their knowledge and expertise to develop smart biomaterials that address essential health concerns. In this sense, this study seeks to instill in students the value of multidisciplinary research in the development of medical devices that regenerate living tissues.

One key strategy to improve Ti bioactivity is the modification of surface properties such as roughness and topography [9]. These surface properties have shown a pivotal role in governing cellular interaction at the material-bone interface. Once the titanium implant is in contact with living tissues, blood proteins adsorb to the implant surface depending upon its physicochemical properties. These proteins, in turn, will interact with cells and guide their cellular processes, resulting in implant osseointegration [10–13].

Conventional surface treatments have been shown to enhance cellular processes by increasing roughness, changing the topography, or adding bioactive molecules, leading to a stronger bone to implant contact (BIC) than polished surfaces [14–17]. Some commercially available surface modifications are sandblasting/acid-etching (SLA) and anodization. SLA consists of the surface bombardment with ceramics and later submerged in strong acids (such as hydrofluoric, nitric and sulfuric acid), while anodization is an electrochemical method where Ti is used as an anode in an electrochemical cell with sodium hydroxide or hydrofluoric or sulfuric acid as electrolytes. The structures created in SLA are random and in the range of micro and nanometers scale, which have shown to promote implant osseointegration [16,18,19]. On the other hand, the anodization process produces ordered and high-aspect-ratio nanotubes, depending on anodization conditions, which has also enhanced the osteoblast response [9,20]. Additionally, multiple studies have used nanotubes as drug reservoirs to deliver growth factors or antibacterial agents to enhance the osteogenic properties of Ti [21–24]. For example, the usage of members of the Bone Morphogenetic Protein family (BMPs) has improved Ti osseointegration in *in vitro* and *in vivo* conditions, highlighting BMP-2 protein as one of the most osteogenic factors used in clinical applications [25–27]. Nevertheless, using SLA or anodized surfaces have encountered several limiting factors regarding the reproducibility of geometrical features, the use of highly toxic reagents or additional steps, which might increase the cost of production and reduce the industry scalability [9,16,28,29]. Therefore, new methods to nanopattern surfaces with high tunability on nanofeatures morphology, size and surface chemistry-independent modification are being intensively investigated. Under this premise, ion irradiation is a scalable industrial method that tailors ion-surface interactions to form reproducible and geometrically interesting nanostructures on the surface in a controlled manner [30,31]. Directed irradiation synthesis (DIS) is an advanced ion irradiation method that uses gradient energetic ion beams to create hierarchical micro/nanostructures in a bottom-up fashion [30,32,33]. When energetic ions collide and interact with the solid, ions transfer energy to the surface atoms. If these atoms have sufficient kinetic energy, they will leave their position in the atomic lattice (sputtering) and create point defects (vacancies and

interstitials). The movement of these defects in the lattice may form complex structures or result in phase changes due to species accumulation in an area. Thus, ion irradiation may result in substantial chemical and morphological changes on the surface [30,34].

DIS shows multiple advantages compared to conventional nanopatterning techniques or new sintering methods, it is a fast process, reliable, with strong capacity to tune small nanofeatures (10 to 100's nm) without the use of masks [29], high temperature [35] or toxic reagents [32,33]. In addition, this bottom-up technique has previously shown the capability to tailor nanofeatures on Ti surfaces keeping the bulk properties stable when using low fluences. This bioactive nanotopography has been shown to modulate cytoskeleton orientation and cell adhesion, as well as cell viability, guiding the tissue regeneration process [32,33].

Based on previous results in our group, in this study, we have characterized the surface properties of DIS-treated titanium samples irradiated using high fluences and different incidence angles and evaluated the effect of combining these active nanotopographies with effective biologics, such as BMP-2, to help elicit a cellular biological response, which may have a synergistic effect in promoting osteoblast differentiation in a BMP-2 responsive cellular model such as C2C12 cells [36]. To the best of our knowledge, this is the first study that does a systematic study using ion-induced surface patterning techniques in synergy with biologics compared with industry-leading anodized and sandblast surface treatment technologies.

2. Materials and Methods

For this purpose, we will first characterize the surface properties (topography, chemistry and wettability) (Figure 1a) and evaluate the effect of the different samples on cell adhesion and spreading (number of filopodia, cell and nucleus shape, vinculin expression, total cells attached), cell viability by measuring cell metabolic activity, osteogenic differentiation and surface mineralization) (Figure 1b).

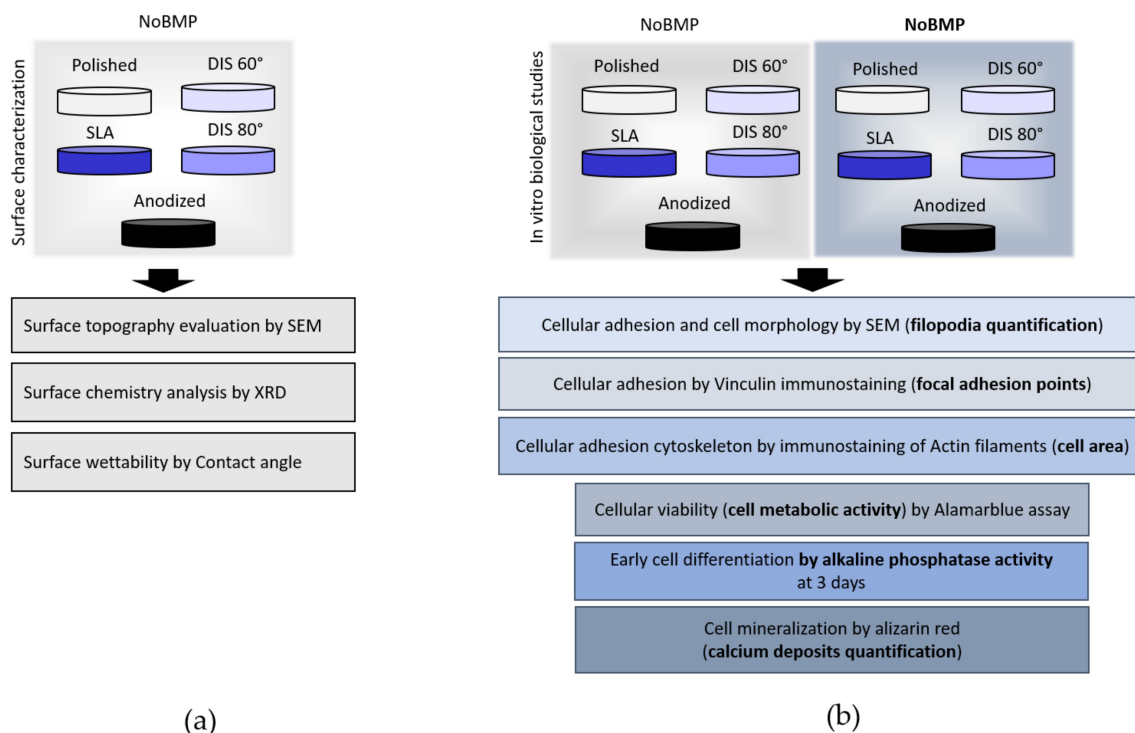


Figure 1. Schematic design of materials and methods of this research study. (a) surface characterization and (b) biological characterization. Abbreviations: Scanning electron microscopy (SEM), X-ray diffraction (XRD), Alkaline Phosphatase (ALP), NoBMP (without BMP-2 protein), BMP (with BMP-2 protein), DIS 60° (Ti6Al4V irradiated using argon ions and 60 incidence angle), DIS 80° (Ti6Al4V irradiated using argon ions and 80 incidence angle), Sandblasted and acid etched Ti6Al4V (SLA), Acid etched and anodized Ti6Al4V (Anodized).

2.1. Titanium Sample Preparation

Titanium alloy samples (Ti4Al6V, area 0.25 cm², Stryker, Kalamazoo, MI, USA) were polished to mirror finished and cleaned before DIS irradiation. The samples were grinded using 320, 1200 and 2400 sandpaper in an Ecomet III grinder (Buehler, Lake Bluff, IL, USA) then were mirror-polished using a ChemoMet cloth (Buehler, Lake Bluff, IL, USA) with a 0.05 µm silica solution (MasterMet, Buehler, Lake Bluff, IL, USA). Afterwards, the samples were ultrasonically cleaned in acetone, isopropanol, ethanol, and water for 15 min each. As controls sandblasted/acid-etched (SLA, commercially pure Ti grade IV, area 0.21 cm²) and acid-etched/anodized (Anodized), area 0.25 cm²) Ti6Al4V surfaces were used. SLA surfaces were provided by Tissue Engineering Group (TEG) of the Complutense University of Madrid, Spain. DIS samples were irradiated with argon ions at 1000 eV of energy and 1×10^{18} ions/cm² using two different incidence angles: 60° and 80° degrees naming the samples DIS 60° and DIS 80°, respectively. All samples were ultrasonically cleaned and autoclaved before using them for the in vitro studies.

2.2. Surface Characterization of Titanium Samples

The surface topography was analyzed by scanning electron microscopy (SEM, S-4800, Hitachi, Tokyo, Japan) at two ranges of magnification: 10 k–22 k to detect microstructures and 70 k–100 k to detect submicron and nanostructures. The surface chemistry was examined by X-ray diffraction (XRD, PANalytical Phillips X'pert MRD system #2, Malvern Panalytical, Malvern, United Kingdom) with Cu K α radiation wavelength ($\lambda = 0.15418$ nm), generated at a voltage of 45 kV and a filament emission of 40 mA. Theta angle (2θ) was collected from $2\theta = 30$ – 80° , with a step size of 0.02° , and the analysis was performed with Origin and Jade software. The surface hydrophilicity was determined by contact angle (CA, Ramé-hart 250 Contact Angle Goniometer, Ramé-hart, Succasunna, NJ, USA) with DROPimage Advanced Software. The sessile method of CA analysis was employed, using 3 µL of deionized water drops to measure the CA of each sample; 4 samples per condition were used for the measurements.

2.3. In Vitro Cell Culture

2.3.1. C2C12 Cell Line

C2C12 cells are multipotent cells that can differentiate, in addition to myotubes, into osteoblasts and adipocytes under specific culture conditions [37]. They have been widely used to study BMP-2 bioactivity since they display low basal BMP signaling activity and show good BMP-2 responsiveness. e.g., expressing bone differentiation markers (early phase such as alkaline phosphatase (ALP) or late-stage such as osteocalcin (OCN)), and inducing the formation of calcium nodules in ascorbic acid, β -glycerol phosphate and dexamethasone rich media [36,38,39]. Murine C2C12 myoblasts were purchased from the American Type Culture Collection (ATCC[®] CRL-1772). This cell line was maintained in Dulbecco's Modified Eagle Medium (DMEM) (ATCC[®] 30-2002[™]) supplemented with 10% Fetal Bovine Serum (FBS) (Invitrogen, Waltham, MA, USA) in a 37 °C, 5% CO₂ incubator. At 80% cellular confluence, cells were trypsinized in 0.25% Trypsin/EDTA (Invitrogen, Waltham, MA, USA). C2C12 passages <20 were cultured in Ti samples at densities of 60,000 cell/cm² (adhesion assay) or 100,000 cell/cm² (viability, osteogenic differentiation and mineralization assay) in 48 well-plates (Corning Costar) with DMEM media, 10% FBS and 3 µg/mL of BMP-2. The cells were initially cultured in 10 µL drops with BMP-2 on Ti surfaces for 4 h to promote cell attachment and then the rest of the media was added (490 µL).

Cellular Adhesion

To determine the combined effect of BMP2 and DIS surface treatment during initial cellular attachment of C2C12, cells were cultured as mentioned above on the different Ti surfaces (DIS 60°, DIS 80°, and polished, SLA, and Anodized as controls). After 4 h, Ti samples were prepared for SEM and confocal laser scanning microscopy. For SEM,

the samples were washed twice with Phosphate-buffered saline (PBS) and fix with 2.5% glutaraldehyde (Sigma, St. Louis, MO, USA) overnight at 4 °C. Then, samples were dehydrated using an ethanol gradient in PBS (30%, 50%, 70%, 80%, 90% and 100%), each step for 15 min. Afterwards, they were critically point dried, sputter with gold-palladium and observed using a scanning electron microscope (JSM-6490LV, Jeol, Tokyo, Japan) at 2 k–3.5 k magnification. For confocal microscopy, the Ti samples were washed twice with PBS and fixed with 5% Formalin (Sigma, MO, USA) for 10 min, permeabilized with 0.1% Triton X-100 (Sigma, St. Louis, MO, USA) for 5 min, washed with 0.01% BSA/PBS and incubated for 30 min at room temperature with Texas red phalloidin (Invitrogen, Waltham, MA, USA) (1:75), DAPI (ThermoFisher, Waltham, MA, USA) (1:1000) and Alexa 647 vinculin (Invitrogen, Waltham, MA, USA) (1:125) to stain actin filaments, nuclei and vinculin, respectively. Finally, the samples were examined via confocal microscopy (Leica SP8 Laser Confocal Microscope Microsystems, Wetzlar, Germany). The number of filopodia, vinculin intensity, total cells, cell area and nucleus area were quantified using FIJI software.

Cell Viability

C2C12 cells were seeded on titanium discs as mentioned above. After 3 days, the Ti samples were incubated for 3 h with Alamarblue (Invitrogen, Waltham, MA, USA) following the manufacturer's recommendations. Briefly, media was removed to avoid counting unattached cells and fresh media with Alamarblue in a 1:10 ratio was added to the wells. Alamarblue is a resazurin-based solution, a cell-permeable compound that upon entering living cells is reduced to resorufin, a fluorescent compound. After incubating the samples in the dark for 3 h, the fluorescence signal was measured using a microplate reader (Synergy HT, BioTek, Winooski, VT, USA) at 530 nm/590 nm Ex/Em.

Evaluation of Cell Differentiation: Alkaline Phosphatase Activity

C2C12 cells were seeded on titanium discs as mentioned above. After 3 days, cells were washed twice with PBS, and lysed by the addition of 100 µL of buffer lysate and subjecting the samples to 3 cycles at −80 °C/37 °C for 30 min. ALP activity was measured according to the manufacturer's instructions using a commercial ALP kit (ab83369, Abcam, Cambridge, MA, USA). ALP hydrolyses phosphate esters in alkaline conditions, generating an organic radical and an inorganic phosphate. This ALP kit uses p-nitrophenyl phosphate (pNPP) as a phosphatase substrate which is dephosphorylated by ALP, generating a yellow compound (p-nitrophenol). The absorbance was measured at 405 nm on a microplate reader (Synergy HT, BioTek, Winooski, VT, USA). ALP enzyme activity was expressed U/L.

Evaluation of Cell Mineralization: Calcium Deposits Production

C2C12 cells were seeded on Ti discs in a 48 well-plate at 37 °C in a 5% CO₂ incubator at a density of 100,000 cell/cm² in DMEM with 10% FBS, 3 µg/mL of BMP-2, 100 nM of dexamethasone (Sigma, St. Louis, MO, USA, USA), 1 mM of β-Glycerophosphate (Sigma, St. Louis, MO, USA) and 50 µg/mL of L-ascorbic acid (Sigma, St. Louis, MO, USA). The media was changed every 2–3 days. After 21 days, the samples were washed with PBS, fixed with 4% formaldehyde for 15 min, stained with 40 mM of alizarin red solution (Sigma, St. Louis, MO, USA) for 30 min and washed 5 times with deionized water to remove the excess of the alizarin red solution. The red deposits were quantified in FIJI. The mineralization percentage (%) was calculated by dividing the area covered by the red deposits to cell culture area times 100.

2.4. Statistical Analysis

All experiments were done in triplicates using two to three samples per condition, except for the confocal and SEM experiments where we examined 3–5 different fields of a sample. Analysis of variance (ANOVA) and Bonferroni's Multiple Comparison Test were used to determine statistically significant differences at 0.05 level of significance by using Origin lab and Graph Prism 5 software.

3. Results and Discussion

3.1. Characterization of Irradiated Titanium Samples

3.1.1. Evaluation of Surface Topography of Irradiated Titanium Samples

Ion irradiation transfers energy and momentum via ion-atom collisions. This results in erosive and diffusive regimes, which drive the surfaces to self-nanopatterned, generating surfaces with attractive topographies [40]. Previous work conducted on Ti alloy and pure titanium (porous scaffolds) revealed that changing the incidence angle, the nanopatterning process was governed by two regimes: diffusion and erosion. At normal incidence angle (0°) and low fluences (ion/cm^2), ion diffusive process predominates, generating short nanoripples and nanorod-like structures. Moving from 0 to 60° , in small or low off-normal angles, there is a combination of diffusive and erosive regimes where ripples and nanorods are combined on the surface, increasing the uniformity of the surface treatment and length. At highly oblique off-normal angles ($\geq 80^\circ$), an erosion regime predominates, in which ions from the source crash and sputter the atoms of the outmost layer of the surface. This complex process showed more elongated nanoripples and no nanorods [32,33]. In this study, we have observed that at higher fluences and off-normal incidence angles, nanoripples have grown in height, turning into nanowalls/nanocones. As observed in Figure 2, scanning electron microscopy (SEM) images of the studied specimens surface topography, DIS 60° generated nanowalls homogeneously distributed on the surface of $16.5 \pm 1 \text{ nm}$ of thickness, and $41.2 \pm 2.9 \text{ nm}$ of spacing distance between nanowalls (white arrow); whereas DIS 80° samples presented nanocone-like structures of a width of $36.7 \pm 9.9 \text{ nm}$ (white arrow) spaced throughout the surface.

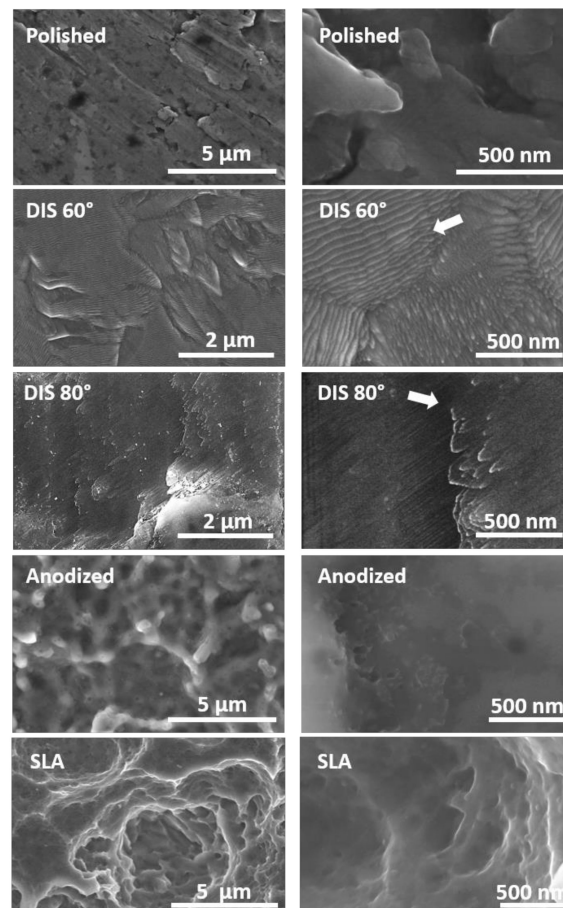


Figure 2. Scanning electron micrographs of modified Ti samples, white arrows indicate nanostructures.

3.1.2. Evaluation of Surface Chemistry and Wettability of Irradiated Titanium Alloy Specimens

Our samples are ($\alpha + \beta$) titanium alloy that contains α stabilizer element aluminum and β stabilizer element vanadium. α phase could be observed using (100), (002) and (101) α peaks. β phase could be observed at (110) β peaks (black arrow). We did not observe any major changes in the α and β phase of the modified DIS Ti samples, which confirms the similar surface crystalline structure of Ti6Al4V modified samples as polished Ti (Figure 3) [41,42]. These surface modifications do not change the bulk crystallographic orientation of Ti (microstructure) due to the low ion penetration around 3–4 nm depth [32,33].

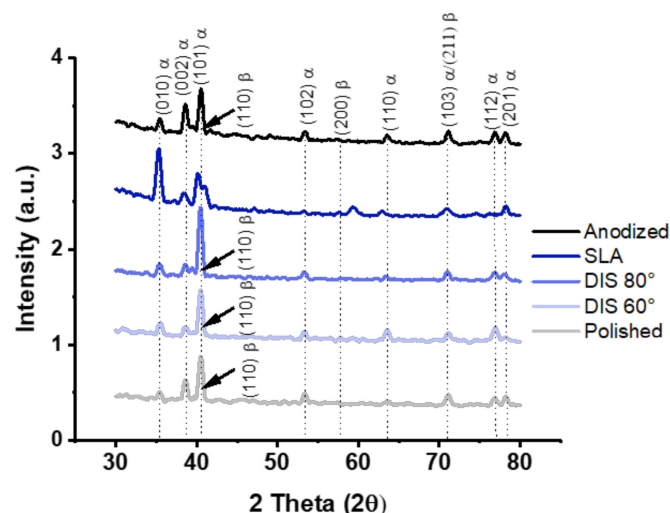


Figure 3. XRD pattern of modified Ti samples. Black arrows indicate (110) β peak.

On the other hand, we did observe a reduction of CA values on DIS samples compared to polished surfaces. DIS surfaces were slightly more hydrophilic than polished Ti even though no statistical differences were detected ($p > 0.05$). It should be noticed that SLA ($40.83 \pm 3.42^\circ$) and Anodized ($20.57 \pm 0.9^\circ$) showed statistical differences with polished and DIS-treated samples. Therefore, SLA and Anodized samples were more hydrophilic surfaces compared to polished or DIS-treated samples which had similar wettability, polished ($79.43 \pm 3.44^\circ$), DIS 60° ($65.33 \pm 3.89^\circ$) and DIS 80° ($71.33 \pm 1.27^\circ$) (Figure 4).

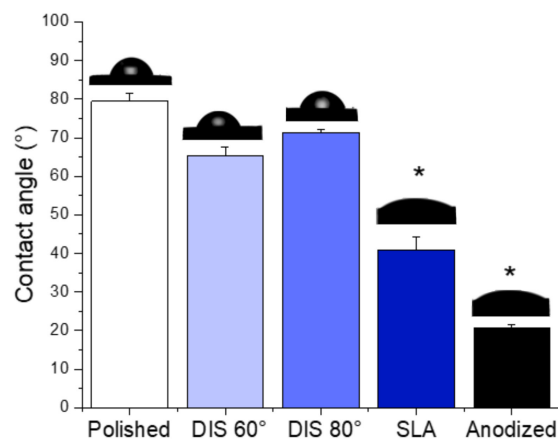


Figure 4. Determination of hydrophilicity/hydrophobicity of Ti samples by contact angle measurement. Mean + SE, N = 3 * p -values < 0.05 compared to polished, DIS 60° and DIS 80° .

3.2. In Vitro Biological Characterization of Titanium Samples

3.2.1. Evaluation of the Cellular Attachment on Irradiated Titanium Samples

After the implantation-derived immune response, mesenchymal stem cells (MSC) migrate to the implant site, where growth factors are released, and start their differentiation process into bone-forming cells [6,43]. In light of this, we evaluated cellular attachment of undifferentiated bone-forming cells 4 h after seeding on the BMP-2 conjugated modified Ti alloy surfaces through the analysis of SEM microphotographs (compiled in Figure 5). We observed the presence of attached cells in all samples. However, SEM images suggested that with the addition of BMP-2, the filopodia number per cell increases, particularly for DIS 80° and Anodized samples and slightly for SLA samples. We observed a 2.25-fold increase on DIS 80° and 0.6-fold increase on Anodized samples compared to their counterpart without BMP-2. However, DIS 80° samples seemed to have more filopodia (39 ± 20 filopodia) compared to the other samples averaging less than 30 filopodia per cell (see Figure 5a,b). Although these results are promising, it will be interesting in future studies to measure the adhesion strength of cells cultured on these surfaces to corroborate this data. Filopodia protrusions are composed of bundles of actin filaments which play a role in the initial cell adhesion, spreading and migration. Cells use filopodia to sense and tether to their surroundings, which require the development of strong tensile forces. As time progresses, these tensile forces will further stabilize the cells, recruiting cell adhesion receptors (integrins) and force-regulating proteins (vinculin, tailin and zyxin), which participate in forming mature adhesions [44–46].

Due to the values observed on titanium surfaces regarding cellular adhesion structures (filopodia prolongations), we decided to evaluate the adhesion process by the immunostaining and quantification of vinculin protein expression. Vinculin protein participates in focal adhesion complexes and plays a fundamental role in cell-cell and cell-matrix interactions and regulates adhesion through binding, polymerizing and remodeling actin fibers [47,48]. Figure 6a shows the confocal images of C2C12 cells, in which vinculin proteins appeared in green, actin in red, and cell nuclei in blue color. Cell number and vinculin intensity from these images were quantified using FIJI software and the results were compiled in Figure 6b. We observed that the addition of BMP-2 increased vinculin expression on cells growing on polished (465%), DIS 80° (200%) and Anodized samples (110%) compared to the samples without BMP-2, although no statistical differences between DIS 80° with BMP-2 and polished BMP-2 were found.

In addition, cell spreading was evaluated through the analysis of the confocal microphotographs (compiled in Figure 7). The cell cytoskeleton, which is composed of actin filaments, was measured to determine the area of the cell (Figure 7a). We observed that the presence of BMP-2 in cells growing on DIS 80° samples showed higher surface area, increasing cellular spreading by 120% compared to its counterpart without the protein, but no statistical differences were found compared to polished samples with BMP-2 (Figure 7b). Although we did not observe significant differences in nucleus area among the different samples, it seemed that the addition of BMP-2 increased the nucleus area of cells cultured on DIS 80° samples (Figure 7c).

Figure 8 shows cell viability results after 3 days of cell culture of all studied surfaces measured by the metabolic activity of C2C12 cells. Percentages of cell viability were calculated using polished without BMP-2 as reference (100%), observing that all surfaces achieved cell viability percentages from 80 to 120%.

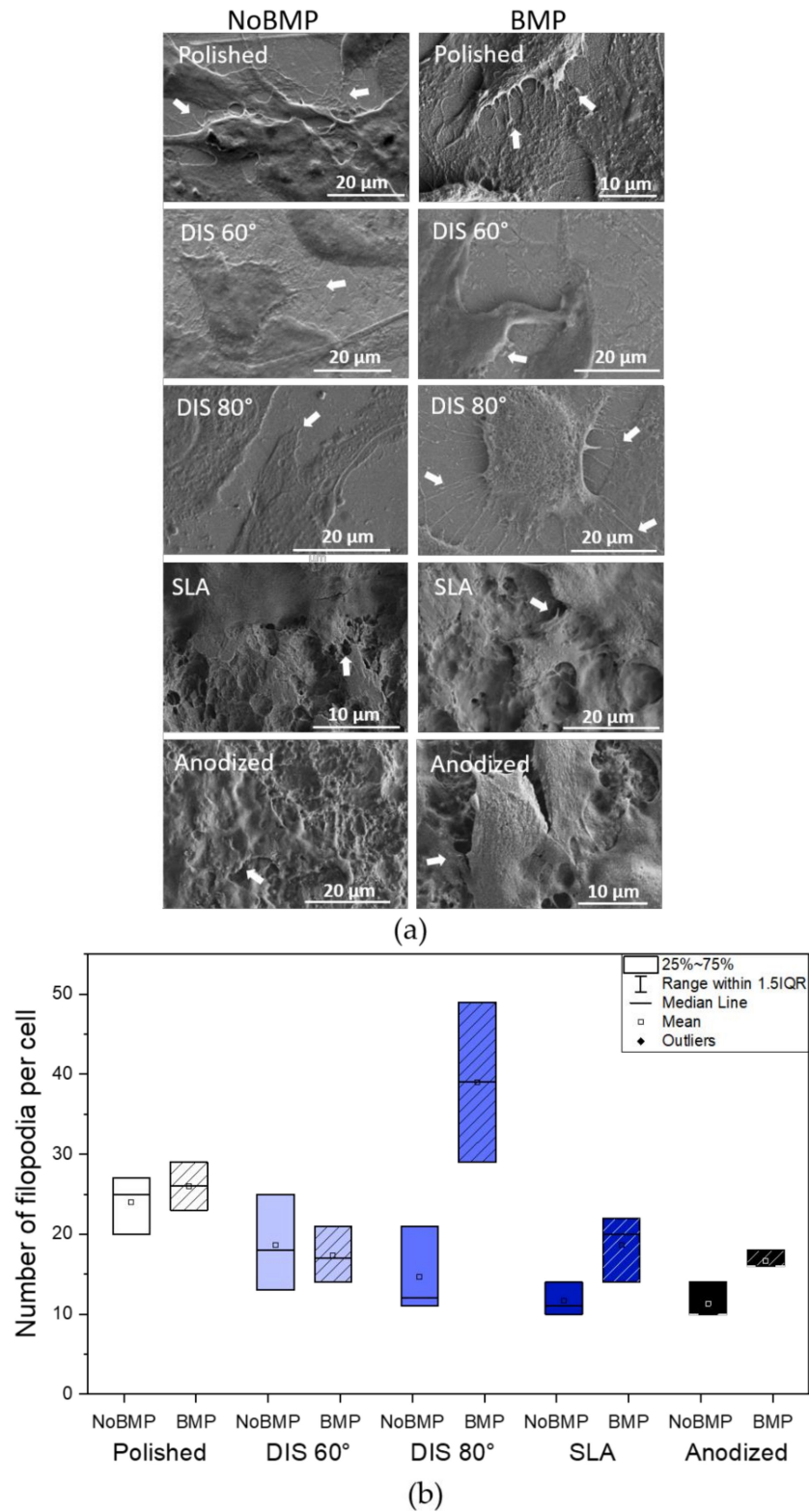
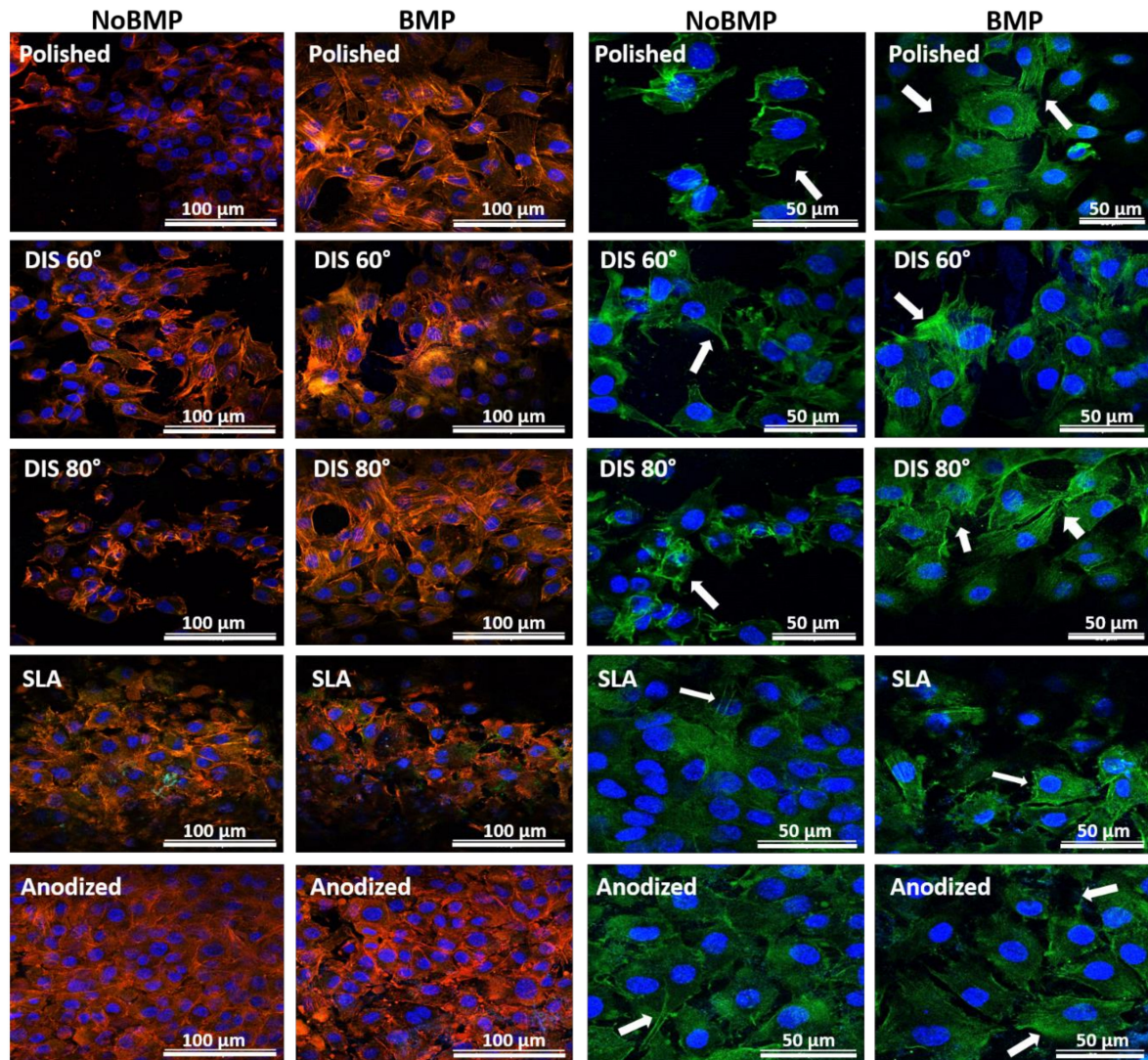
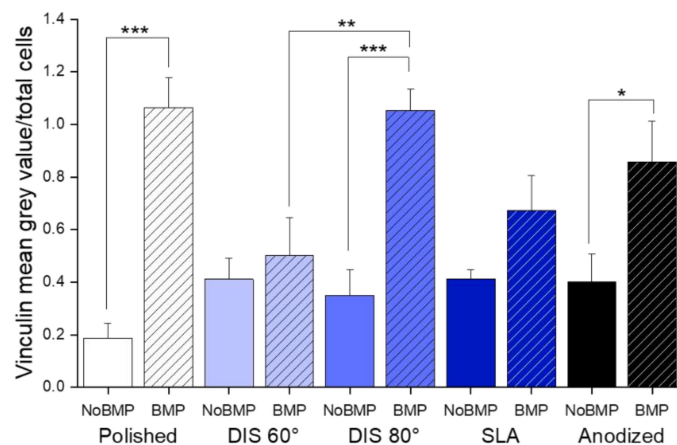


Figure 5. Evaluation of cell morphology on Ti alloy surfaces with and without the incorporation of BMP-2. (a) SEM micrographs of C2C12 cultured on modified Ti samples for 4 h, white arrows indicate filopodia prolongations (b) Filopodia number quantification. Median and IQR, N = 3 fields.



(a)



(b)

Figure 6. Determination of cellular attachment. (a) Confocal microscopy images of C2C12 cells cultured on Ti samples with and without the incorporation of BMP-2. Vinculin protein was stained green (white arrows), actin filaments in red and cell nuclei in blue; (b) Vinculin mean grey value of samples with and without the incorporation of BMP-2 normalized to total cells. Mean + SE N = 5 fields, *** $p < 0.001$, ** $p < 0.001$, * $p < 0.05$.

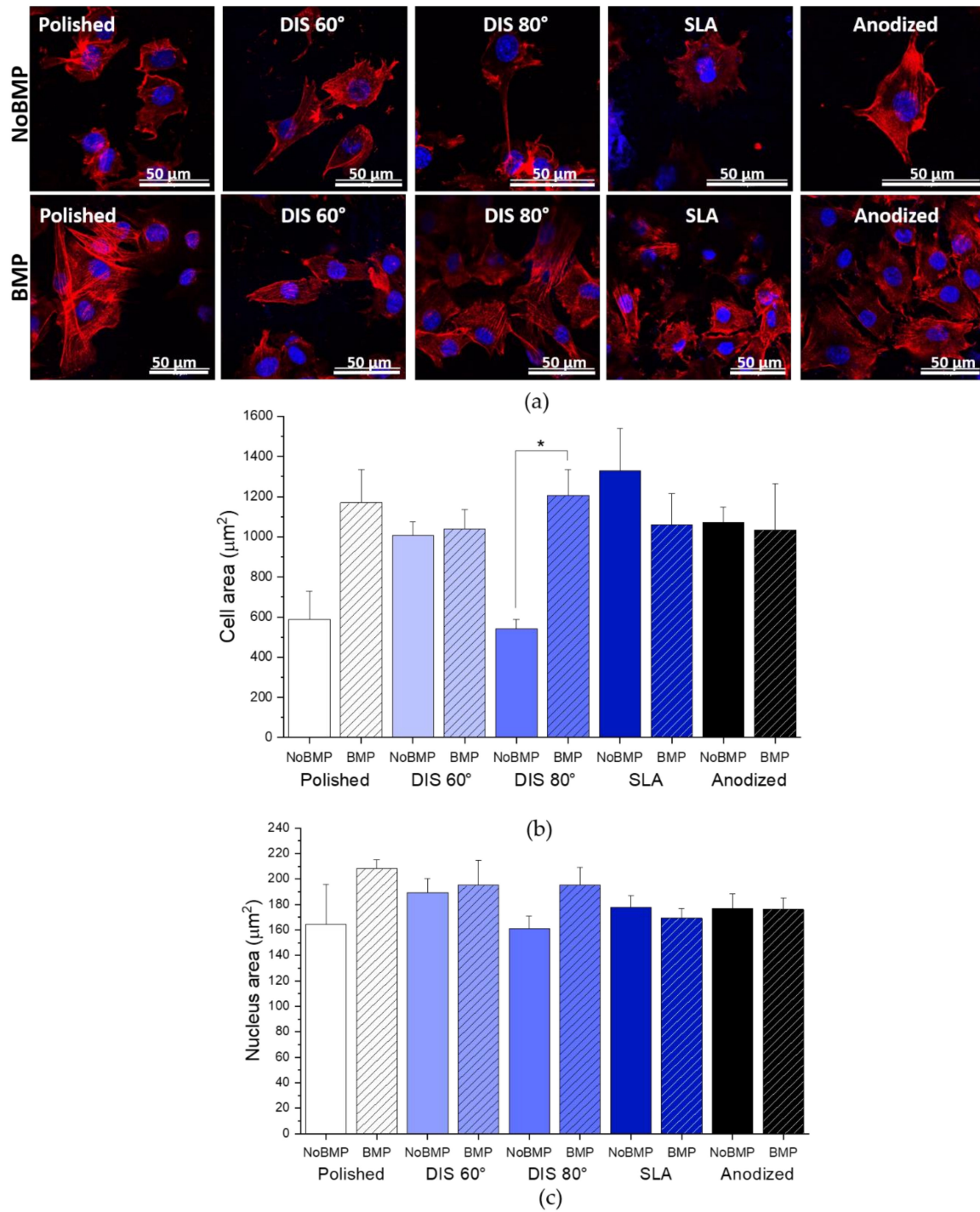


Figure 7. Cell spreading. (a) Confocal microscopy of C2C12 cultured on Ti samples with and without the incorporation of BMP-2. The cytoskeleton actin filaments were stained red and nuclei blue; (b) Cell area measured by FIJI software. Mean + SE, N = 3 fields, * $p < 0.05$; (c) Nucleus area. Mean + SE, N < 3 fields.

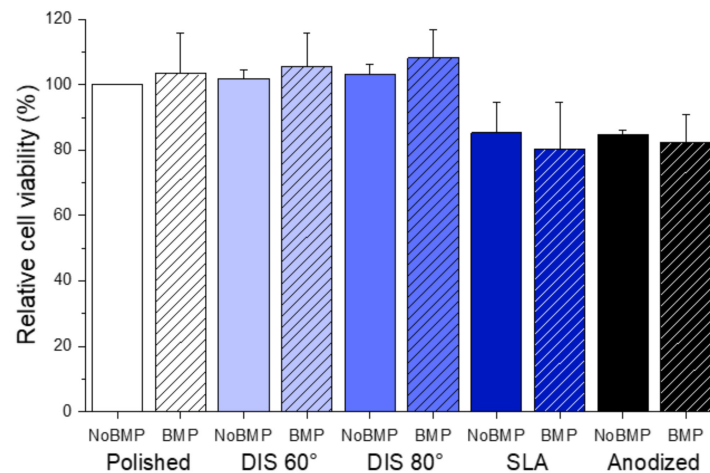


Figure 8. Relative C2C12 viability on Ti samples with and without the incorporation of BMP-2 normalized to polished without BMP-2 after 3 days in culture. Mean + SE, N = 3.

Integrins α and β -subunit are linked to the actin cytoskeleton via adaptor proteins (talin and vinculin). Integrins agglomerate and form focal adhesions, which translate mechanical stimuli into biochemical signals that will start gene expression either by activating signaling pathways, such as extracellular-signal-regulated kinase (ERK)/mitogen-activated protein kinase (MAPK) or through actomyosin contractility, which will distort the shape of the nucleus and allow the translocation of transcription factors [47–49]. Fourel and collaborators observed an increase in $\beta 3$ integrin expression in C2C12 cultured on soft polymeric films with matrix-bound BMP-2, which promoted cell spreading and adhesion [50]. BMP-2 enhancement of C2C12 cellular adhesion has also been reported in hydroxyapatite and magnesium surfaces by Huang and collaborators [51]. In this study, we used nanopatterned metallic substrates, which might serve as BMP-2 nanoreservoirs, promoting localized BMP-2 signaling. We observed an increase in vinculin intensity and changes in cell area in surfaces with BMP-2, particularly in DIS 80° treated surfaces. Although we did not measure integrin expression, the vinculin and cell spreading results suggest that integrin-mediated signaling is involved in this process and could explain the changes we observed in cellular attachment and cell fate.

Moreover, topographical features have been found to influence cell attachment [13,49]. For example, Pan and collaborators evaluated the behavior of MSC on a macropore/nanowire structure fabricated via vacuum plasma spraying and etching with sodium hydroxide (NaOH), which mimics bone hierarchical microenvironment. These cells were elongated and spread in multiple directions with well-developed focal adhesions. This led to an increase in cytoskeletal tension and yes-associated protein (YAP) activity and nuclear translocation. YAP is a member of the Hippo Signaling pathways that shuttles between the cytoplasm and the nucleus under specific physical cues, e.g., stiffness and topography, acting as a promoter for osteogenic transcription factors; thus, inducing MSC differentiation [52]. Other structures such as nanotubes (diameters of 10 nm and 30 nm), which have spacings of less than 50 nm provide an effective length promoting integrin clustering/focal contact formation and increasing detachment forces [53,54]. It is hypothesized that this is caused by the structures matching the integrin diameters (10 nm) [55]. Alternatively, this phenomenon might be caused by an increase in surface contact area to which more integrins can bind to. For example, Babchenko and collaborators have found that nanopatterned surfaces with nanocones, which were densely packed and distributed homogeneously on the surface, increased vinculin signaling and promoted focal adhesion kinase (FAK) activation in osteoblastic-like cells (Saos-2) [56,57]. Considering this, the dimensions of our nanostructures could further improve integrin-mediated adhesion and traction forces; and thus, their involvement in mechanotransduction pathways. Integrin expression and its role on cell morphology and behavior is the focus of a future study

which will include cells at different stages of osteogenic differentiation and different stages of cellular adhesion.

Other factors that influence osteoblast cell spreading and proliferation are surface texturing/patterning [8,58]. Although we did not measure roughness (Sa) in this study, similar Ar⁺ irradiation conditions (with lower fluence 2.5×10^{17} ions/cm²) were performed on titanium alloy and showed Sa of 10 to 50 nm reaching higher values on SLA (49 nm) [32]. However, it will be interesting in further studies to correlate these measurements with the DIS conditions used in this study.

3.2.2. Evaluation of Osteogenic Differentiation and Mineralization on Irradiated Titanium Samples

Generally, there are three major stages during MSC osteogenic differentiation: differentiation, matrix maturation, and mineralization. First, attached MSC will differentiate into osteoprogenitor cells expressing Runt-related transcription factor 2 (Runx2), Distal-less homeobox 5 (Dlx5) and Osterix (Osx). Once committed to an osteogenic lineage, these cells (preosteoblasts) will express ALP and collagen I (Col I) and eventually will differentiate into mature osteoblasts, expressing and secreting Col I, OCN, and osteopontin (OPN), which form the matrix. Afterwards, ALP will aid in the mineralization process by releasing phosphate ions, which will be combined with calcium to produce hydroxyapatite. In mouse models, the mineralization phase peaks at 14–21 days [59–62]. In C2C12, ALP is expressed by stimulating the cells with 300 ng/mL of BMP-2 after 2–3 days in culture, which induces their osteogenic differentiation and inhibits myotube formation [38,63]. From previous studies and what has been established in the literature, BMP-2 UdeA optimal concentration was 3 µg/mL to detect significant ALP production after 3 days of C2C12 cell culture [64].

For this purpose, we cultured BMP-2 and C2C12 cells directly on modified Ti alloy surfaces and evaluated the osteogenic differentiation and mineralization. We observed statistical differences in ALP activity produced by cells on Ti surfaces with BMP-2 *versus* without BMP-2 due to the intrinsic osteoinductive effect of BMP-2. We observed an increase in ALP production for DIS 80° (265%), Anodized (195%) and SLA samples (190%), yet we did not observe statistical differences among the different samples with BMP-2. This fact suggests that BMP-2 plays a more dominant role in cell differentiation than the surface nanotopography. Nevertheless, it should be noticed the slightly higher ALP activity on cells growing on DIS 80° surfaces with BMP-2 compared to the other samples with BMP-2, which suggests a possible synergistic effect between the nanopatterned irradiated surface at 80° and BMP-2s (Figure 9a). This synergistic effect might be similar to the one MSCs face in their native environment, where they have physical and biological cues, leading to their differentiation into bone cells. On the other hand, the late phase of osteoblast differentiation or cell mineralization phase is characterized by the presence of calcium and phosphate deposits, which form hydroxyapatite and collagen fiber production. Through Alizarin red staining of free calcium nodules, we could determine the extent of the C2C12 cell mineralization process on Ti surfaces in the presence of mineralization media [39]. DIS 80° and Anodized surfaces with BMP-2 showed a greater mineralization area after 21 days in cell culture compared to other samples, particularly DIS 80° with BMP-2 increased the percentage of calcium nodules by 329% compared to polished samples with BMP-2 (Figure 9b). The differences between DIS-based modified surfaces and BMP-2 mineralization results could, in fact, still be within the variance as the statistical sample was limited.

Surface treatment can influence the adsorption of bone extracellular matrix proteins such as BMP-2 and modulate cell behavior. For instance, Xiao and collaborators evaluated BMP-2 adsorption on polished, etched and anodized Ti surfaces. They found that etched samples had the highest BMP-2 absorption, yet the protein changed its conformation and reduced its bioactivity in MSC in the long term, in contrast to BMP-2 adsorbed on anodized samples [65]. They also studied the synergistic effect of BMP-2/fibronectin adsorption on these surfaces and observed that it promoted MSC spreading and osteoblast differentiation [66]. These results agree with those observed in our study in which DIS 80° in

the presence of BMP-2 showed the highest levels of vinculin expression (FAK components) and cell spreading (cell area). Nevertheless, future studies are needed to evaluate how our surfaces modulate protein conformation, adsorption, bioactivity at different concentrations and timepoints and their effects on cellular behavior.

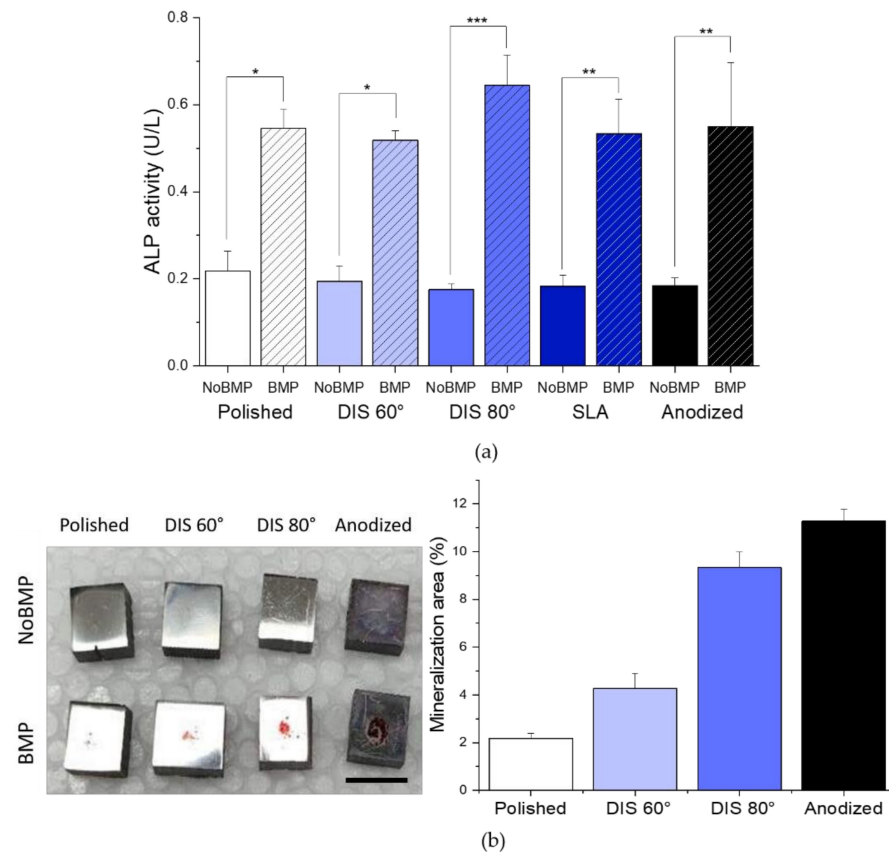


Figure 9. C2C12 osteoblast differentiation and mineralization. (a) ALP production after 3 days on Ti samples with and without the incorporation of BMP-2. Mean + SE, N = 3, *** $p < 0.001$, ** $p < 0.001$, * $p < 0.05$; (b) Cell mineralization. Cell culture with mineralization media on Ti sample with and without the incorporation of BMP-2, black bar indicates 0.5 cm (left panel), quantification of mineralization area compared to the culture area of samples with BMP-2 (right panel). Mean + SD, N = 3 fields.

Researchers have observed that cells can respond to nanopatterns of less than 13 nm in height or orthogonal or hexagonal patterns of nanopits with diameters from 35 to 200 nm [67]. Nanopits of 22 nm promote osteogenic gene expression via integrin signaling [68]. Our results agree with other studies using different nanopatterning techniques, which stimulate bone formation by targeting integrin signaling [69–71] yet DIS presents many advantages over these methods. By modulating DIS irradiation parameters, we can generate reproducible and scalable nanopatterns directly on the material in a short amount of time (usually a few minutes) without using toxic chemicals that pose health risks or require extra steps to discard them. Future studies will focus on evaluating integrin-mediated bone formation on these surfaces.

BMP-2 controlled delivery is one of the main challenges in bone tissue engineering as uncontrolled drug release can cause serious side effects such as ectopic bone formation, bone reabsorption and hematomas in soft tissues [72]. Currently, these and other growth factors can be tethered to the implant surface via physisorption or covalent binding to control their release. Physical adsorption relies on electrostatic interactions, hydrogen bonding, or hydrophobic interactions. In covalent binding, the substrate is treated with plasmas, chemical etching and surface coatings to functionalize the surface. Also, bioconju-

gation reactions such as amidation, esterification and click reactions through carbodiimides, silanes, mussel-inspired bioconjugation have been used [73,74]. Another strategy is to encapsulate growth factors in scaffolds, e.g., titania nanotubes, to control the release of BMP-2 and induce bone formation [21,73]. Therefore, it will be interesting in the future to evaluate the functionalization of these surfaces via ion irradiation with non-inert gases (nitrogen and oxygen) to generate functional groups in which BMP-2 can be tether to and control its release.

4. Conclusions

The combination of growth factors (BMP-2) and active nanotopographies (nanocones and nanowalls-like structures) have demonstrated a synergy in cell adhesion, differentiation and mineralization of a non-osteoblastic cell lineage (C2C12 cells). The following findings can be drawn:

1. DIS allowed the design of nanostructures on titanium alloys surfaces, resulting in nanocones and nanowalls of size below 50 nm by changing the incidence angle from 60 to 80 degrees with high fluences.
2. The crystalline structure of DIS samples was unmodified; and although no statistical differences were observed in terms of wettability, DIS samples seemed more hydrophilic than polished samples.
3. The presence of BMP-2 plays an important role in cellular adhesion and spreading. In this study, BMP-2 addition seemed to increase filopodia number per cell and vinculin expression in most surfaces and cell spreading on DIS 80° and polished surfaces compared to surfaces without BMP-2. However, surface topography or nanopatterning by itself does not contribute significantly to these processes, except by increasing slightly vinculin expression in DIS 80° nanocone-patterned surfaces.
4. DIS 80° nanocone-patterned surfaces in conjunction with BMP-2 increase almost 1.2-fold cell spreading and 2-fold vinculin expression, reaching values similar to polished samples with BMP-2. Moreover, we observed a 2.25-fold increase in the number of filopodia per cells (39 ± 20) in these surfaces compared to all surfaces with or without BMP-2, suggesting a synergistic effect in cell adhesion when we combine DIS 80° treatment with BMP-2.
5. Cell differentiation and mineralization, determined by ALP activity and calcium nodules formation, respectively, were enhanced in the presence of BMP-2 for all samples. In particular, we observed that this effect was more pronounced on DIS 80° and Anodized samples with BMP-2 (>2-fold increase in ALP activity compared to their counterparts without BMP-2 and >3.3-fold increase in cell mineralization compared to polished samples with BMP-2).
6. Finally, the nanocone-like structures generated at an incidence angle of 80° in combination with BMP-2 have shown a stronger synergistic effect in modulating cellular processes when compared to DIS 60° and polished observing this nanocone topography more suitable to improve cellular interactions. Thus, DIS treatment in conjunction with BMP-2 may improve Ti implants osseointegration by guiding cell differentiation toward bone formation.

Author Contributions: Conceptualization, project administration, supervision, methodology, J.P.A., J.J.P., R.M., E.P., J.F.A., N.B., Y.T., J.A.R.-O., A.C. and A.M.-R., Investigation, formal analysis, validation, A.M.-R. and A.C. Discussion and writing—original draft preparation, all the authors. All authors have read and agreed to the published version of the manuscript.

Funding: This work was supported by the Ministry of Science and Innovation of Spain under the grant PID2019-109371GB-I00, by the Junta de Andalucía–FEDER (Spain) through the Project Ref. US-1259771, Colciencias (Departamento Administrativo de Ciencia, Tecnología e Innovación) under the grant COL-13-2-16 and University of Antioquia Master's Scholarship fund. The BMP-2 production work was supported by AM LTDA and Transferencia Tecnológica from University of Antioquia under the grant CODI-UdeA # 2017-18192.

Data Availability Statement: Not applicable.

Acknowledgments: The authors would like to thank University of Antioquia and Colciencias for the funding, Sandra Arias and Camilo Jaramillo for the DIS treatment and Viviana Posada for taking some of the SEM micrographs as well as professors Luz Marina Restrepo, Junes Villarraga and Gabriel Bedoya for their guidance. Surface characterization was performed in Frederick Seitz Materials Research Lab and all the in vitro experiments were conducted in Micro and Nanotechnology Lab in UIUC.

Conflicts of Interest: The authors declare no conflict of interest.

References

- de Witte, T.M.; Fratila-Apachitei, L.E.; Zadpoor, A.A.; Peppas, N.A. Bone tissue engineering via growth factor delivery: From scaffolds to complex matrices. *Regen. Biomater.* **2018**, *5*, 197–211. [CrossRef]
- Jin, W.; Chu, P.K. Orthopedic implants. In *Encyclopedia of Biomedical Engineering*; Elsevier: Amsterdam, The Netherlands, 2019; pp. 425–439. [CrossRef]
- Kirmanidou, Y.; Sidira, M.; Drosou, M.E.; Bennani, V.; Bakopoulou, A.; Tsouknidas, A.; Michailidis, N.; Michalakis, K. New Ti-alloys and surface modifications to improve the mechanical properties and the biological response to orthopedic and dental implants: A review. *BioMed Res. Int.* **2016**, *2016*, 1–21. [CrossRef] [PubMed]
- Shah, F.A.; Thomsen, P.; Palmquist, A. Osseointegration and current interpretations of the bone-implant interface. *Acta Biomater.* **2019**, *84*, 1–15. [CrossRef] [PubMed]
- Spriano, S.; Yamaguchi, S.; Baino, F.; Ferraris, S. A critical review of multifunctional titanium surfaces: New frontiers for improving osseointegration and host response, avoiding bacteria contamination. *Acta Biomater.* **2018**, *79*, 1–22. [CrossRef] [PubMed]
- Ramazanoglu, M.; Oshi, Y. Osseointegration and bioscience of implant surfaces—Current concepts at bone-implant interface. In *Implant Dentistry—A Rapidly Evolving Practice*; Turkyilmaz, I., Ed.; InTech: Rijeka, Croatia, 2011. Available online: <http://www.intechopen.com/books/implant-dentistry-a-rapidly-evolving-practice/osseointegration-and-bioscience-of-implant-surfaces-current-concepts-at-bone-implant-interface> (accessed on 4 October 2014).
- Landgraber, S.; Jäger, M.; Jacobs, J.J.; Hallab, N.J. The pathology of orthopedic implant failure is mediated by innate immune system cytokines. *Mediat. Inflamm.* **2014**, *2014*, 1–9. [CrossRef] [PubMed]
- Durmus, N.G.; Webster, T.J. Nanostructured titanium: The ideal material for improving orthopedic implant efficacy? *Nanomedicine* **2012**, *7*, 791–793. [CrossRef] [PubMed]
- Mansoorianfar, M.; Khataee, A.; Riahi, Z.; Shahin, K.; Asadnia, M.; Razmjou, A.; Hojjati-Najafabadi, A.; Mei, C.; Orooji, Y.; Li, D. Scalable fabrication of tunable titanium nanotubes via sonoelectrochemical process for biomedical applications. *Ultrason. Sonochem.* **2020**, *64*, 104783. [CrossRef]
- Beutner, R.; Michael, J.; Schwenzer, B.; Scharnweber, D. Biological nano-functionalization of titanium-based biomaterial surfaces: A flexible toolbox. *J. R. Soc. Interface* **2009**, *7*, S93–S105. [CrossRef]
- Feller, L.; Jadwat, Y.; Khammissa, R.A.G.; Meyerov, R.; Schechter, I.; Lemmer, J. Cellular responses evoked by different surface characteristics of intraosseous titanium implants. *BioMed Res. Int.* **2015**, *2015*, 1–8. [CrossRef] [PubMed]
- Lavenus, S.; Louarn, G.; Layrolle, P. Nanotechnology and dental implants. *Int. J. Biomater.* **2010**, *2010*, 1–9. [CrossRef]
- Aminuddin, N.I.; Ahmad, R.; Akbar, S.A.; Pinguan-Murphy, B. Osteoblast and stem cell response to nanoscale topographies: A review. *Sci. Technol. Adv. Mater.* **2016**, *17*, 698–714. [CrossRef] [PubMed]
- Bosshardt, D.D.; Chappuis, V.; Buser, D. Osseointegration of titanium, titanium alloy and zirconia dental implants: Current knowledge and open questions. *Periodontol. 2000* **2017**, *73*, 22–40. [CrossRef] [PubMed]
- Gittens, R.A.; Scheideler, L.; Rupp, F.; Hyzy, S.L.; Geis-Gerstorfer, J.; Schwartz, Z.; Boyan, B.D. A review on the wettability of dental implant surfaces II: Biological and clinical aspects. *Acta Biomater.* **2014**, *10*, 2907–2918. [CrossRef] [PubMed]
- Jemat, A.; Ghazali, M.J.; Razali, M.; Otsuka, Y. Surface modifications and their effects on titanium dental implants. *BioMed Res. Int.* **2015**, *2015*, 1–11. [CrossRef] [PubMed]
- Civantos, A.; Martínez-Campos, E.; Ramos, V.; Elvira, C.; Gallardo, A.; Abarrategi, A. Titanium coatings and surface modifications: Toward clinically useful bioactive implants. *ACS Biomater. Sci. Eng.* **2017**, *3*, 1245–1261. [CrossRef]
- Souza, J.C.; Sordi, M.B.; Kanazawa, M.; Ravindran, S.; Henriques, B.; Silva, F.S.; Aparicio, C.; Cooper, L.F. Nano-scale modification of titanium implant surfaces to enhance osseointegration. *Acta Biomater.* **2019**, *94*, 112–131. [CrossRef] [PubMed]
- İzmir, M.; Ercan, B. Anodization of titanium alloys for orthopedic applications. *Front. Chem. Sci. Eng.* **2019**, *13*, 28–45. [CrossRef]
- Gao, A.; Hang, R.; Bai, L.; Tang, B.; Chu, P.K. Electrochemical surface engineering of titanium-based alloys for biomedical application. *Electrochim. Acta* **2018**, *271*, 699–718. [CrossRef]
- Tao, B.; Deng, Y.; Song, L.; Ma, W.; Qian, Y.; Lin, C.; Yuan, Z.; Lu, L.; Chen, M.; Yang, X.; et al. BMP2-loaded titania nanotubes coating with pH-responsive multilayers for bacterial infections inhibition and osteogenic activity improvement. *Colloids Surfaces B Biointerfaces* **2019**, *177*, 242–252. [CrossRef]
- Li, Y.; Song, Y.; Ma, A.; Li, C. Surface immobilization of TiO₂ nanotubes with bone morphogenetic protein-2 synergistically enhances initial Preosteoblast adhesion and osseointegration. *BioMed Res. Int.* **2019**, *2019*, 1–12. [CrossRef] [PubMed]

23. Wigmosta, T.B.; Popat, K.C.; Kipper, M.J. BMP -2 delivery from polyelectrolyte multilayers enhances osteogenic activity on nanostructured titania. *J. Biomed. Mater. Res. Part A* **2020**. [[CrossRef](#)] [[PubMed](#)]
24. Oliveira, W.F.; Arruda, I.R.; Silva, G.M.; Machado, G.; Coelho, L.C.; Correia, M.T. Functionalization of titanium dioxide nanotubes with biomolecules for biomedical applications. *Mater. Sci. Eng. C* **2017**, *81*, 597–606. [[CrossRef](#)] [[PubMed](#)]
25. Teng, F.Y.; Tai, I.C.; Ho, M.L.; Wang, J.W.; Weng, L.W.; Wang, Y.J.; Wang, M.W.; Tseng, C.C. Controlled release of BMP-2 from titanium with electrodeposition modification enhancing critical size bone formation. *Mater. Sci. Eng. C* **2019**, *105*, 109879. [[CrossRef](#)]
26. Wu, C.; Lu, H. Smad signal pathway in BMP-2-induced osteogenesis a mini review. *J. Dent. Sci.* **2008**, *3*, 13–21.
27. Teng, F.Y.; Chen, W.C.; Wang, Y.L.; Hung, C.C.; Tseng, C.C. Effects of osseointegration by bone morphogenetic protein-2 on titanium implants in vitro and in vivo. *Bioinorg. Chem. Appl.* **2016**, *2016*, 1–9. [[CrossRef](#)]
28. Kang, Y.; Ren, X.; Yuan, X.; Ma, L.; Xie, Y.; Bian, Z.; Zuo, J.; Wang, X.; Yu, Z.; Zhou, K.; et al. The effects of combined micron-scale surface and different nanoscale features on cell response. *Adv. Mater. Sci. Eng.* **2018**, *2018*, 1–9. [[CrossRef](#)]
29. Greer, A.I.; Goriainov, V.; Kanczler, J.; Black, C.R.; Turner, L.A.; Meek, R.M.; Burgess, K.; MacLaren, I.; Dalby, M.J.; Oreffo, R.O.; et al. Nanopatterned titanium implants accelerate bone formation in vivo. *ACS Appl. Mater. Interfaces* **2020**, *12*, 33541–33549. [[CrossRef](#)]
30. Allain, J.P.; Shetty, A. Unraveling atomic-level self-organization at the plasma-material interface. *J. Phys. D Appl. Phys.* **2017**, *50*, 283002. [[CrossRef](#)]
31. Averback, R. Ion-irradiation studies of cascade damage in metals. *J. Nucl. Mater.* **1982**, *108–109*, 33–45. [[CrossRef](#)]
32. Civantos, A.; Barnwell, A.; Shetty, A.R.; Pavón, J.J.; El-Atwani, O.; Arias, S.L.; Lang, E.; Reece, L.M.; Chen, M.; Allain, J.P. Designing nanostructured Ti6Al4V bioactive interfaces with directed irradiation synthesis toward cell stimulation to promote host-tissue-implant integration. *ACS Biomater. Sci. Eng.* **2019**, *5*, 3325–3339. [[CrossRef](#)]
33. Civantos, A.; Allain, J.P.; Pavón, J.J.; Shetty, A.; El-Atwani, O.; Walker, E.; Arias, S.L.; Gordon, E.; Rodríguez-Ortiz, J.A.; Chen, M.; et al. Directed irradiation synthesis as an advanced plasma technology for surface modification to activate porous and “as-received” titanium surfaces. *Metals* **2019**, *9*, 1349. [[CrossRef](#)]
34. Krashennnikov, A.V.; Nordlund, K. Ion and electron irradiation-induced effects in nanostructured materials. *J. Appl. Phys.* **2010**, *107*, 071301. [[CrossRef](#)]
35. Ghasali, E.; Baghchesaraee, K.; Orooji, Y. Study of the potential effect of spark plasma sintering on the preparation of complex FGM/laminated WC-based cermet. *Int. J. Refract. Met. Hard Mater.* **2020**, *92*, 105328. [[CrossRef](#)]
36. de Gorter, D.J.; van Dinther, M.; Dijke, P.T. Measurement of constitutive activity of BMP type I receptors. *Methods Enzymol.* **2010**. [[CrossRef](#)]
37. Mancini, A.; El Bounkari, O.; Norrenbrock, A.F.; Scherr, M.; Schaefer, D.; Eder, M.; Banham, A.H.; Pulford, K.; Lyne, L.; Whetton, A.D.; et al. FMIP controls the adipocyte lineage commitment of C2C12 cells by downmodulation of C/EBPalpha. *Oncogene* **2006**, *26*, 1020–1027. [[CrossRef](#)]
38. Katagiri, T.; Yamaguchi, A.; Komaki, M.; Abe, E.; Takahashi, N.; Ikeda, T.; Rosen, V.; Wozney, J.M.; Fujisawa-Sehara, A.; Suda, T. Bone morphogenetic protein-2 converts the differentiation pathway of C2C12 myoblasts into the osteoblast lineage. *J. Cell Biol.* **1994**, *127*, 1755–1766. [[CrossRef](#)]
39. Hidaka, Y.; Chiba-Ohkuma, R.; Karakida, T.; Onuma, K.; Yamamoto, R.; Fujii-Abe, K.; Saito, M.M.; Yamakoshi, Y.; Kawahara, H. Combined effect of midazolam and bone morphogenetic protein-2 for differentiation induction from C2C12 myoblast cells to osteoblasts. *Pharmaceutics* **2020**, *12*, 218. [[CrossRef](#)]
40. Mishra, I.; Joshi, S.R.; Majumder, S.; Manna, A.K.; Varma, S. Low energy ion irradiation of TiO₂ (110)—Understanding evolution of surface morphology and scaling studies. *Radiat. Eff. Defects Solids* **2016**, *171*, 594–605. [[CrossRef](#)]
41. Xue, L. Laser Consolidation—A rapid manufacturing process for making net-shape functional components. In *Advances in Laser Materials Processing*; Elsevier: Amsterdam, The Netherlands, 2018; pp. 461–505. [[CrossRef](#)]
42. Pederson, R.; Babushkin, O.; Skystedt, F.; Warren, R. Use of high temperature X-ray diffraction to study phase transitions and thermal expansion properties in Ti-6Al-4V. *Mater. Sci. Technol.* **2003**, *19*, 1533–1538. [[CrossRef](#)]
43. Albertini, M.; Yagüe, M.-A.F.; Lázaro, P.; Herrero-Climent, M.; Rios-Santos, J.-V.; Bullon, P.; Gil Mur, F.J. Advances in surfaces and osseointegration in implantology. Biomimetic surfaces. *Med. Oral Patol. Oral Cir. Bucal* **2015**, *20*, e316–e325. [[CrossRef](#)] [[PubMed](#)]
44. Hu, W.; Wehrle-Haller, B.; Vogel, V. Maturation of filopodia shaft adhesions is upregulated by local cycles of lamellipodia advancements and retractions. *PLoS ONE* **2014**, *9*, e107097. [[CrossRef](#)]
45. Jacquemet, G.; Hamidi, H.; Ivaska, J. Filopodia in cell adhesion, 3D migration and cancer cell invasion. *Curr. Opin. Cell Biol.* **2015**, *36*, 23–31. [[CrossRef](#)]
46. Mattila, P.K.; Lappalainen, P. Filopodia: Molecular architecture and cellular functions. *Nat. Rev. Mol. Cell Biol.* **2008**, *9*, 446–454. [[CrossRef](#)]
47. Bays, J.L.; DeMali, K.A. Vinculin in cell–cell and cell–matrix adhesions. *Cell. Mol. Life Sci.* **2017**, *74*, 2999–3009. [[CrossRef](#)]
48. Kechagia, J.Z.; Ivaska, J.; Roca-Cusachs, P. Integrins as biomechanical sensors of the microenvironment. *Nat. Rev. Mol. Cell Biol.* **2019**, *20*, 457–473. [[CrossRef](#)]
49. Bertrand, A.A.; Malapati, S.H.; Yamaguchi, D.T.; Lee, J.C. The intersection of mechanotransduction and regenerative osteogenic materials. *Adv. Healthc. Mater.* **2020**, *9*, 2000709. [[CrossRef](#)]

50. Fourel, L.; Valat, A.; Faurobert, E.; Guillot, R.; Bourrin-Reynard, I.; Ren, K.; Lafanechère, L.; Planus, E.; Picart, C.; Albiges-Rizo, C. β 3 integrin-mediated spreading induced by matrix-bound BMP-2 controls Smad signaling in a stiffness-independent manner. *J. Cell Biol.* **2016**, *212*, 693–706. [[CrossRef](#)] [[PubMed](#)]
51. Huang, B.; Yuan, Y.; Li, T.; Ding, S.; Zhang, W.; Gu, Y.; Liu, C. Facilitated receptor-recognition and enhanced bioactivity of bone morphogenetic protein-2 on magnesium-substituted hydroxyapatite surface. *Sci. Rep.* **2016**, *6*, 24323. [[CrossRef](#)]
52. Pan, H.; Xie, Y.; Zhang, Z.; Li, K.; Hu, D.; Zheng, X.; Fan, Q.; Tang, T. YAP-mediated mechanotransduction regulates osteogenic and adipogenic differentiation of BMSCs on hierarchical structure. *Colloids Surf. B Biointerfaces* **2017**, *152*, 344–353. [[CrossRef](#)]
53. Park, J.; Bauer, S.; Von Der Mark, K.; Schmuki, P. Nanosize and vitality: TiO₂Nanotube diameter directs cell fate. *Nano Lett.* **2007**, *7*, 1686–1691. [[CrossRef](#)]
54. Selhuber-Unkel, C.; Erdmann, T.; López-García, M.; Kessler, H.; Schwarz, U.; Spatz, J. Cell adhesion strength is controlled by intermolecular spacing of adhesion receptors. *Biophys. J.* **2010**, *98*, 543–551. [[CrossRef](#)]
55. Jäger, M.; Jennissen, H.P.; Dittrich, F.; Fischer, A.; Köhling, H.L. Antimicrobial and osseointegration properties of nanostructured titanium orthopaedic implants. *Materials* **2017**, *10*, 1302. [[CrossRef](#)]
56. Babchenko, O.; Kromka, A.; Hruska, K.; Kalbacova, M.H.; Broz, A.; Vanecek, M. Fabrication of nano-structured diamond films for SAOS-2 cell cultivation. *Phys. Status Solidi A* **2009**, *206*, 2033–2037. [[CrossRef](#)]
57. Kalbacova, M.; Broz, A.; Babchenko, O.; Kromka, A. Study on cellular adhesion of human osteoblasts on nano-structured diamond films. *Phys. Status Solidi B* **2009**, *246*, 2774–2777. [[CrossRef](#)]
58. Ferreira, M.R.W.; Fernandes, R.R.; Assis, A.F.; Dernowsek, J.A.; Passos, G.A.; Variola, F.; Bombonato-Prado, K.F. Oxidative nanopatterning of titanium surface influences mRNA and MicroRNA expression in human alveolar bone osteoblastic cells. *Int. J. Biomater.* **2016**, *2016*, 1–15. [[CrossRef](#)]
59. Capulli, M.; Paone, R.; Rucci, N. Osteoblast and osteocyte: Games without frontiers. *Arch. Biochem. Biophys.* **2014**, *561*, 3–12. [[CrossRef](#)]
60. James, A.W. Review of signaling pathways governing MSC osteogenic and adipogenic differentiation. *Scientifica* **2013**, *2013*, 1–17. [[CrossRef](#)]
61. Karperien, M.; Roelen, B.A.; Poelmann, R.E.; Groot, A.C.G.-D.; Hierck, B.P.; DeRuiter, M.C.; Meijer, D.; Gibbs, S. Tissue formation during embryogenesis. *Tissue Eng.* **2015**. [[CrossRef](#)]
62. Blair, H.C.; Larrouture, Q.C.; Li, Y.; Lin, H.; Beer-Stoltz, D.; Liu, L.; Tuan, R.S.; Robinson, L.J.; Schlesinger, P.H.; Nelson, D.J. Osteoblast differentiation and bone matrix formation in vivo and in vitro. *Tissue Eng. Part B Rev.* **2017**, *23*, 268–280. [[CrossRef](#)]
63. Vaes, B.L.T.; Dechering, K.J.; Feijen, A.; Hendriks, J.M.A.; Lefèvre, C.; Mummery, C.L.; Olijve, W.; Van Zoelen, E.J.J.; Steegenga, W.T. Comprehensive microarray analysis of bone morphogenetic protein 2-induced osteoblast differentiation resulting in the identification of novel markers for bone development. *J. Bone Miner. Res.* **2002**, *17*, 2106–2118. [[CrossRef](#)]
64. Mesa-Restrepo, A.; Alzate, J.F.; Patiño-Gonzalez, E. Bone morphogenetic protein 2: Heterologous expression and potential in bone regeneration. *Actual. Biol.* **2021**, *43*, 1–10, in press. [[CrossRef](#)]
65. Xiao, M.; Biao, M.; Chen, Y.; Xie, M.; Yang, B.; Xiao, M.; Biao, M.; Chen, Y.; Xie, M.; Yang, B. Regulating the osteogenic function of rhBMP 2 by different titanium surface properties. *J. Biomed. Mater. Res. Part A* **2016**, *104*, 1882–1893. [[CrossRef](#)]
66. Biao, M.N.; Chen, Y.M.; Xiong, S.B.; Wu, B.Y.; Yang, B.C. Synergistic effects of fibronectin and bone morphogenetic protein on the bioactivity of titanium metal. *J. Biomed. Mater. Res. Part A* **2017**, *105*, 2485–2498. [[CrossRef](#)] [[PubMed](#)]
67. Cavalcanti-Adam, E.A.; Aydin, D.; Hirschfeld-Warneken, V.C.; Spatz, J.P. Cell adhesion and response to synthetic nanopatterned environments by steering receptor clustering and spatial location. *HFSP J.* **2008**, *2*, 276–285. [[CrossRef](#)] [[PubMed](#)]
68. Rosa, A.; Kato, R.; Raucci, L.C.; Teixeira, L.; De Oliveira, F.; Bellesini, L.; De Oliveira, P.; Hassan, M.; Beloti, M. Nanotopography drives stem cell fate toward osteoblast differentiation through α 1 β 1 integrin signaling pathway. *J. Cell. Biochem.* **2014**, *115*, 540–548. [[CrossRef](#)]
69. Lotz, E.M.; Olivares-Navarrete, R.; Berner, S.; Boyan, B.D.; Schwartz, Z. Osteogenic response of human MSCs and osteoblasts to hydrophilic and hydrophobic nanostructured titanium implant surfaces. *J. Biomed. Mater. Res. Part A* **2016**, *104*, 3137–3148. [[CrossRef](#)] [[PubMed](#)]
70. Fernández-Yagüe, M.; Antoñanzas, R.P.; Roa, J.J.; Biggs, M.; Gil, F.J.; Pegueroles, M. Enhanced osteoconductivity on electrically charged titanium implants treated by physicochemical surface modifications methods. *Nanomed. Nanotechnol. Biol. Med.* **2019**, *18*, 1–10. [[CrossRef](#)] [[PubMed](#)]
71. Lopes, H.B.; Freitas, G.P.; Elias, C.N.; Tye, C.; Stein, J.L.; Stein, G.S.; Lian, J.B.; Rosa, A.L.; Beloti, M.M. Participation of integrin β 3 in osteoblast differentiation induced by titanium with nano or microtopography. *J. Biomed. Mater. Res. Part A* **2019**, *107*, 1303–1313. [[CrossRef](#)]
72. El Bialy, I.; Jiskoot, W.; Nejadnik, M.R. Formulation, delivery and stability of bone morphogenetic proteins for effective bone regeneration. *Pharm. Res.* **2017**, *34*, 1152–1170. [[CrossRef](#)]
73. Dang, M.; Saunders, L.; Niu, X.; Fan, Y.; Ma, P.X. Biomimetic delivery of signals for bone tissue engineering. *Bone Res.* **2018**, *6*, 1–12. [[CrossRef](#)] [[PubMed](#)]
74. Wang, Z.; Wang, Z.; Lu, W.W.; Zhen, W.; Yang, D.; Peng, S. Novel biomaterial strategies for controlled growth factor delivery for biomedical applications. *NPG Asia Mater.* **2017**, *9*, e435. [[CrossRef](#)]